Catalysis and Temperature Dependence on the Formation of ZnO Nanoparticles and of Zinc Acetate Derivatives Prepared by the Sol−Gel Route

Miriam S. Tokumoto,[†,‡] Sandra H. Pulcinelli,[†] Celso V. Santilli,[†] and Valérie Briois*[,‡]

UNESP, Instituto de Quimica, P.O. Box 355, 14800-900 Araraquara-SP, Brazil, and LURE, Centre Universitaire Paris-Sud, BP 34, 91898 Orsay Cedex, France

Received: July 25, 2002; In Final Form: October 22, 2002

The chemical and structural nature of powders prepared from the zinc acetate-derived precursor using the sol−gel route is discussed. The influence of the synthesis temperature and of the hydrolytic catalyst on the structural features of the powder is focused on the basis of X-ray powder diffraction (XRPD) and extended X-ray absorption fine structure (EXAFS) measurements and complemented with density and thermoanalysis (TG-DTA) results. EXAFS and XRPD results show that no-washed nanoparticulate powders are composed of a mixture of ZnO (wurtzite), zinc acetate, and zinc hydroxyacetate. The latter has a layered structure typical of hydroxy double salts (HDS). The main component of no-washed powders is always unreacted zinc acetate solid but the relative amount of the zinc-based compounds depends on the nature of the hydrolytic catalyst, hydrolysis ratio, and of synthesis temperature. According to the proportion of the three zinc-based compounds, three families of powders could be distinguished. The amount of ZnO nanoparticles (1.6 ± 0.6 nm) decreases as the synthesis temperature increases, as the hydrolysis ratio decreases, or by changing from basic to acid catalysis. This finding suggests that the formation of zinc compounds is controlled by the equilibrium between hydrolysis−condensation and complexation−reprecipitation reactions.

1. Introduction

For the past 10 years, research on quantum size semiconductor particles has increased enormously due to their exciting novel optical and electrical properties.[1] Among the techniques of preparation available for these systems, the sol−gel route is very attractive because it is relatively easy to carry out and allows us to produce large quantities of materials. Furthermore, the morphology of particles can be tailored by the relative rate of hydrolysis and condensation reactions.[2] The major problem of the sol−gel route is the control of these reaction rates, which are generally too fast, resulting in the formation of precipitates with a high degree of structural disorder.[2,3] The strategy frequently used to reduce the hydrolysis−condensation rate is the modification of reactivity of precursors by formation of complexed species with strong ligands such as carboxylic acids, β-diketones, and allied derivatives.[3]

The sol−gel method proposed by Spanhel and Anderson[4] in 1991 is commonly used to obtain ZnO nanometer-sized particles, to prepare nanoparticulate films with strong visible luminescence properties.[5] From structural EXAFS data, and IR and UV−vis measurements carried out in solution, we have recently shown[6] that the $Zn_4O(CH_3COO)_6$ tetrameric species[7] is the precursor formed in the first steps of the Spanhel and Anderson route.[4] This precursor is based on a tetrahedron of four Zn^{2+} containing an oxygen, each Zn^{2+} being coordinated tetrahedrally by oxygen peripheral bidentate acetate ligands.[7] It is structurally close to ZnO and its transformation into ZnO could proceed by substitution of peripheral bidentate acetate ligands by hydrolyzable groups followed by subsequent oxolation. It was outlined that nanoparticles obtained by this sol−gel route are not pure ZnO nanocrystals and that the presence of acetate groups on the surface of particles plays a dominant role in the luminescence properties of the so-obtained materials.[8−10] In particular, Sakohara et al.[10] attributed the observed luminescence properties to unidentate acetate groups bonded on the surface of the ZnO particles. Otherwise, the choice of acid or basic catalysis and the temperature was pointed out as playing a key role on the rates of the hydrolysis−condensation reaction and on the equilibrium concentration of dissolved Zn^{2+} species, leading to changes in the size and shape of ZnO-based nanoparticles.[11]

Despite these results of prime importance for film preparation and potential applications, little is known about the chemical and structural nature of the solid particles obtained from the zinc acetate sol−gel route proposed by Spanhel and Anderson.[4] This work reports a systematic structural study of powders prepared by a sol−gel route faintly adapted from the one proposed by Spanhel and Anderson. In particular, we describe the effect of different catalysts and temperature of hydrolysis on the structure and proportion of phases present in dried powders.

2. Experimental Section

2.1. Sample Preparation. The preparation of colloidal suspensions was based on the method proposed by Spanhel and Anderson[4] and briefly described in ref 11. As the experimental procedure is of paramount importance to controlling the chemical nature of powders obtained by hydrolysis, we detail the preparation herein. The procedure consists of two major steps: (1) preparation of the precursor and (2) hydrolysis of the precursor to form the colloidal particles.

The zinc precursor was prepared from zinc acetate, $Zn(CH_3COO)_2 \cdot 2H_2O$ (noted above $ZnAc_2 \cdot 2H_2O$) from Synth and

* Corresponding author. Fax: 33 1 64 46 41 48. E-mail: briois@lure.u-psud.fr.
† UNESP, Instituto de Quimica.
‡ LURE, Centre Universitaire Paris-Sud.

10.1021/jp0217381 CCC: $25.00
Published on Web 12/17/2002

absolute ethanol. A 0.1 mol L^{-1} ethanolic zinc acetate solution was refluxed for 3 h at 80 °C under magnetic stirring. The flask was fitted with a condenser and a $CaCl_2$ trap to avoid moisture exposure. The refluxed solution so obtained is transparent and was stored at ≈4 °C to prevent further precipitation. This solution so-prepared was used as the precursor solution. Structural characterizations[6] carried out in solution have identified the precursors as being the $Zn_4O(CH_3COO)_6$ tetrameric species (noted above Zn_4OAc_6).

Lithium hydroxide, succinic acid, and glacial acetic acid were used as catalysts to hydrolyze the precursor. Hydrolysis of precursors was also carried out without further addition of catalyst or with water. The molar ratios of hydrolysis, defined as $A = [H^+]/[Zn^{2+}]$ for acid conditions, $B = [OH^-]/[Zn^{2+}]$ for basic conditions, and $N = [H_2O]/[Zn^{2+}]$ for neutral conditions, and the temperature of the reaction bath were varied depending on the catalysts used. Because of the importance of water content for the hydrolysis process, careful attention has been paid to controlling addition of extra water. On one hand, absolute ethanol and glacial acetic acid were stored after opening of the bottles on molecular sieves in order to maintain the water content below 0.1 vol %. On the other hand, solid reactants were kept in a vacuum desiccator. It has been checked that moisture contamination of solids was under the detection limit of thermoanalysis measurements. The catalyst was added to the precursor solution under magnetic stirring at 4 °C (into an ultrasonic bath for powdered catalysts, i.e., LiOH). After complete dissolution, the solution was put into a thermostated reaction bath. The hydrolysis time was varied depending on the time evolution of the turbidity reported elsewhere;[11] typically it varies from 30 to 240 min. The precipitates were separated from the solution after sedimentation by removal of the supernatant ethanolic solution and dried at 50 °C. All of the solids were characterized before being washed. Some of these powders were also characterized after washing with distilled water and drying in a vacuum at room temperature.

Crystalline zinc oxide (Prolabo), zinc acetate ($ZnAc_2 \cdot 2H_2O$) (Synth), and the hydroxy double salt $Zn_5(OH)_8(OCOCH_3)_2 \cdot 2H_2O$, labeled hereafter Zn-HDS, were used as standard compounds. Zn-HDS was prepared at room temperature by the addition of an aqueous NaOH solution (0.1 mol L^{-1}) to a zinc acetate solution (0.1 mol L^{-1}) at up to OH/Zn = 1 under magnetic stirring, as reported in ref 12. The precipitated powder was isolated, washed, and dried in a vacuum at room temperature. The structure of the sample so obtained was checked by XRPD, which is similar to the ones reported by Morioka et al.[12]

2.2. Thermoanalysis and Density Measurements. Simultaneous thermogravimetric (TG) and differential thermoanalysis (DTA) of dried powders were measured from room temperature to 800 °C under synthetic air flux, with 20 °C min^{-1} heating rate, by using a SDT2960 (TA Instruments) apparatus. The powder density was measured at 25 °C, with a helium picnometer (Acupic- Micromeritics).

2.3. EXAFS and X-ray Powder Diffraction Measurements. The extended X-ray absorption fine structure (EXAFS) measurements were made at LURE using the DCI storage ring (1.85 GeV, 300 mA). The data were collected at the Zn K edge (9659 eV), at room temperature, on the EXAFS IV spectrometer, using a Si(111) double-crystal monochromator. Detection was done in transmission mode using two ionization chambers filled with air. Samples were ground and mixed with graphite before being pressed into pellets. The quantity of powdered samples was determined in order to obtain edge jumps in transmission mode of about $\Delta\mu x \approx 1$. The X-ray powder diffraction (XRPD) measurements were performed on dried samples with a Siemens D5000 diffractometer, using a graphite monochromatized Cu Kα radiation.

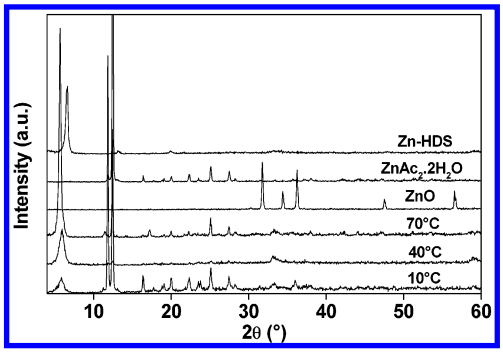

Figure 1. Comparison of the XRPD patterns of the precipitates obtained by LiOH catalysis ($B = 0.1$) at 10, 40, and 70 °C with the XRPD patterns of the standard compounds: ZnO, $ZnAc_2 \cdot 2H_2O$, and $Zn_5(OH)_8(OCOCH_3)_2 \cdot 2H_2O$ (Zn-HDS).

2.4. EXAFS Data Analysis. The EXAFS treatment was performed by using the "EXAFS pour le MAC" program developed by Michalowicz,[13] and the main lines of the procedure are summarized here. After atomic absorption removal based on cubic spline function and normalization, the $k^3 \cdot \chi(k)$ weighted EXAFS signal was Fourier transformed to R (distance) space, using the 3.4−15 $Å^{-1}$ Kaiser apodization window with $\tau = 3$. Among the three standard compounds used in this work, only zinc oxide (with its almost regular tetrahedron of oxygen atoms as first coordination shell[14]) is a suitable reference model for phase and amplitude function extraction. The contribution of the first shell of oxygen neighbors for all the samples was extracted by a back Fourier transform in R space and then fitted using experimental phase and amplitude functions extracted from the ZnO reference. This was done back-transforming the first peak of its Fourier transform (FT) and setting $N_{Zn-O} = 4$, $R =$ 1.98 Å, and $\sigma = 0.07$ Å.[14] The contribution of the Zn nearest neighbors was fitted only for ZnO nanoparticles by using FeFF phase and amplitude functions[15] extracted from the ab initio calculation of the ZnO structure. The FeFF functions were checked on the ZnO reference back-transforming the second peak of its Fourier transform and setting $N_{Zn-Zn} = 12$, R = 3.23 Å, and $\sigma = 0.125$ Å. The reliability of the fit performed in the single scattering approximation is given by the value of the residual function ρ, which relates the experimental (χ_{exp}) and calculated (χ_{calc}) EXAFS functions by

$$\rho = \frac{\sum_i (\chi^i_{exp}(k_i) - \chi^i_{calc}(k_i))^2}{\sum_i (\chi^i_{exp}(k_i))^2} \quad (1)$$

3. Results

Figure 1 compares the diffraction patterns for the precipitates prepared with LiOH as catalyst at different temperatures with the diffraction patterns of the reference compounds, ZnO, $ZnAc_2 \cdot 2H_2O$, and Zn-HDS. Any of the samples presents a diffraction pattern characterized alone by the diffraction peaks of ZnO. The samples are identified as a mixture of ZnO, $ZnAc_2 \cdot 2H_2O$, and Zn-HDS phases. This feature is also observed in the diffraction patterns of powders prepared in the presence of other catalysts considered in this study. The Zn-HDS compound belongs to the same class of layered materials as $Zn_5(OH)_8(NO_3)_2 \cdot 2H_2O$,[16] $Zn_5(OH)_8Cl_2 \cdot H_2O$,[17] and $Zn_5(OH)_6(CO_3)_2$.[18] These structures, often called hydroxy double salt (HDS) structures, are characterized by sheets of composition $[Zn_3^{oct}(OH)_8$-

TABLE 1: Structural Parameters for the First Coordination Sphere of Zinc Derived from the EXAFS Analysis of Samples Prepared from Basic Catalysis by LiOH at Different Temperatures

T (°C)	Family	N_{Zn-O}	R(Å)	σ(Å)	ρ (%)
10	I	3.7 ± 0.2	2.01 ± 0.02	0.09 ± 0.02	0.38
40	II	3.7 ± 0.2	2.02 ± 0.02	0.09 ± 0.02	0.21
		3.8 ± 0.2	2.16 ± 0.02	0.12 ± 0.02	
50	II	3.7 ± 0.2	2.02 ± 0.02	0.09 ± 0.02	0.22
		1.9 ± 0.1	2.18 ± 0.02	0.10 ± 0.02	
70	III	3.2 ± 0.2	2.02 ± 0.02	0.08 ± 0.02	0.20
		2.1 ± 0.1	2.15 ± 0.02	0.12 ± 0.02	

$Zn_2^{tetr}(H_2O)_2]^{2+}$ in which zinc atoms occur in both octahedral and tetrahedral coordination. The octahedrons are involved into brucite type layers with 25% of the octahedral positions unoccupied. Above and below the unoccupied octahedral sites, two zinc ions per formula unit occupy the tetrahedral positions. These layered HDS structures present a characteristic peak at low angle (<10°) due to (00l) reflections corresponding to the interlayer distances. This peak can be used as a fingerprint of the acetate Zn-HDS structure and is observed in most of the samples. We note that the position of this peak changes with the catalyst used in the hydrolysis (neutral, acid, and basic) and for a given catalyst is generally shifted at lower angular values when the temperature is increased, indicating a subsequent increase of the interlamellar distance of the layered Zn-HDS compound. The presence of acetate-based compounds such as $ZnAc_2 \cdot 2H_2O$ and Zn-HDS is in agreement with previous infrared characterizations, which clearly evidenced acetate and zinc acetate vibrations.[11] The number of bands and their relative intensities characteristic of the different phases change with the synthesis conditions (catalyst and temperature).

Figures 2a and 2b present the EXAFS spectra and corresponding FT of the precipitates prepared with LiOH as basic catalyst at different temperatures and compared to ZnO, $ZnAc_2 \cdot 2H_2O$, and Zn−HDS references. The first peak of FTs, labeled Zn−O, is related to the first oxygen coordination shell around Zn. A second intense peak, labeled Zn−Zn, is observed for ZnO, Zn-HDS, and some precipitates. It corresponds to the contribution of Zn nearest neighbors around Zn. Structural parameters resulting from the least-squares fitting procedure of the first peaks of the different FTs are reported in Table 1. By comparison with the EXAFS spectra of the three reference compounds, the different powders were classified into three families of precipitates.

Family I. This family possesses as a typical EXAFS spectrum the one obtained with LiOH catalyst at 10 °C. The EXAFS oscillations are clearly in phase with those of the ZnO reference, attesting to the formation of ZnO particles. All the peaks characteristic of the ZnO structure (until 6 Å) are evidenced on the FT of samples of Family I but with reduced intensities compared to the ZnO reference.

Family II. The EXAFS spectra of powders prepared at $T =$ 40 and 50 °C are characteristic of the second family of compounds. The EXAFS oscillations are in phase with those of the Zn-HDS reference. The FTs present a second peak broader than the one characterizing powders of Family I. This indicates a larger distribution of Zn second nearest neighbors distances around Zn for the compounds of Family II.

Family III. The third family of powders displays as a typical feature a relatively unstructured spectrum like the one obtained at $T =$ 70 °C. This EXAFS spectrum looks like that of $ZnAc_2 \cdot 2H_2O$. Their FTs are, consequently, characterized by a second peak with a smaller amplitude compared to the FTs of samples of Families I and II.

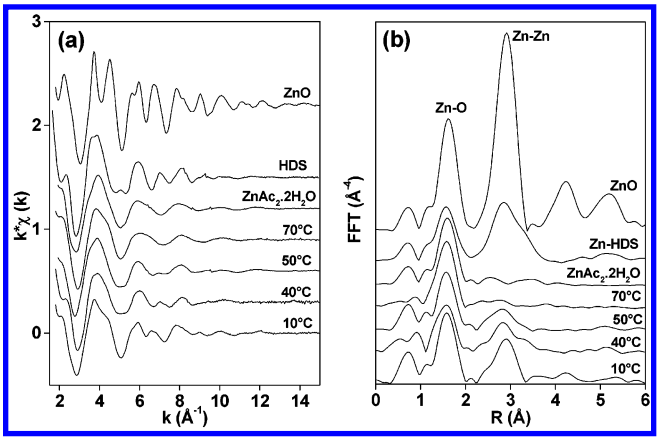

Figure 2. (a) EXAFS spectra of the precipitates obtained by LiOH catalysis ($B = 0.1$) at 10, 40, 50, and 70 °C compared to the EXAFS spectra of the standard compounds: ZnO, $ZnAc_2 \cdot 2H_2O$, and $Zn_5(OH)_8(OCOCH_3)_2 \cdot 2H_2O$ (Zn-HDS) and (b) corresponding FT of the EXAFS signals displayed in (a).

Figures 3a and 3b show the relative mass loss (TG) and differential thermal analysis (DTA) curves corresponding to the reference compounds and some typical samples of Families I, II, and III presented in Figure 2. The amount of residue of 65 wt % observed for acetate Zn-HDS reference is in agreement which the complete conversion of Zn-HDS to ZnO, that would lead to 66 wt %. For the $ZnAc_2 \cdot 2H_2O$ commercial compound the 25 wt % of residue is lower than the expected value (37 wt %) for complete conversion into ZnO. It is due to a volatilization of a significant part of zinc derivatives species observed during thermal decomposition of zinc acetate under dynamic atmosphere.[19] The TG curves of samples of Families I, II, and III show values of residue intermediary to those of $ZnAc_2 \cdot 2H_2O$ and Zn-HDS, characterizing the mixture of phases. The presence of the $ZnAc_2 \cdot 2H_2O$ in the mixture can be distinguished by the three endothermic processes taking place during heating to 350 °C, corresponding to dehydration ($T_{max} \approx 110$ °C), melting of anhydrous salt ($T_{max} \approx 255$ °C), and evaporation of zinc species ($T_{max} \approx 340$ °C).[7] These two later processes are practically absent in the Zn-HDS compound, while the dehydration shows a doublet endothermic effect at 100−115 °C, associated with the elimination of hydration water and hydroxyl groups. These mains features of simultaneous TG-DTA curves allow us to recognize the presence of $ZnAc_2 \cdot 2H_2O$ in the sample hydrolyzed at 10 °C and a mixture of this compound with Zn-HDS, in the powders prepared at 40 and 70 °C. The weight loss due to the elimination of hydroxyl groups is more pronounced in the sample prepared at 40°C, indicating a major amount of acetate Zn-HDS in this sample. These results are in agreement with the qualitative interpretation of EXAFS data shown in Figure 2.

The left and the right side of Figure 4 display the EXAFS spectra and corresponding Fourier transforms (FT) of the powders prepared with different catalysts at various temperatures. As with LiOH, for most of the used catalyst, we can observe a clear modification of the local order around Zn when the temperature of hydrolysis is changed. The classification of the different samples obtained on the basis of EXAFS fingerprints is given in Table 2. The fingerprints used to identify compounds of Family I are the pronounced shoulders on the first two EXAFS oscillations (circles on the different spectra mark them). The fingerprint used for the Family II is either the presence of the small resonance at 7 $Å^{-1}$ in the $k \cdot \chi(k)$ EXAFS or the slope breaking off observed in the second EXAFS

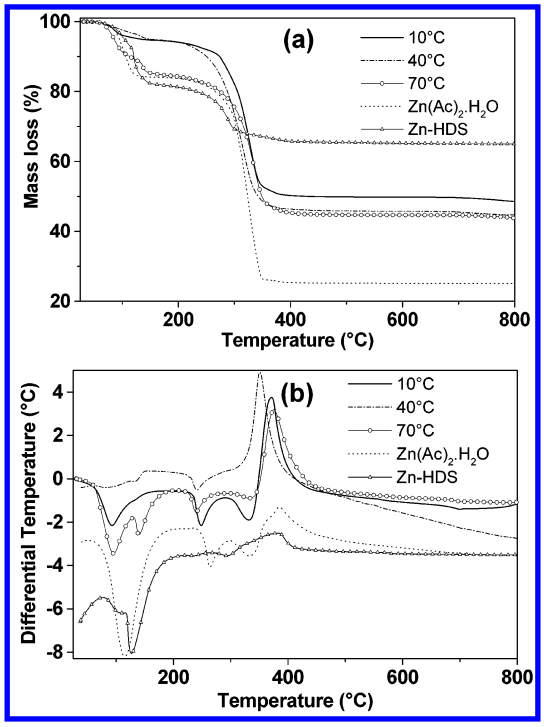

Figure 3. (a) Thermogravimetric and (b) DTA curves for the precipitates obtained by LiOH catalysis ($B = 0.1$) at 10, 40, and 70 °C compared to the curves of the standard compounds: $ZnAc_2 \cdot 2H_2O$ and $Zn_5(OH)_8(OCOCH_3)_2 \cdot 2H_2O$ (Zn-HDS). For sake of clarity, the DTA curves for the standard compounds were shifted downward.

oscillation around 6.5 $Å^{-1}$. These features are marked on the spectra by stars.

Figures 5a and 5b present the EXAFS spectra and corresponding Fourier transforms (FT) of some of the powders prepared from LiOH catalysis belonging to Families I and II after washing with distilled water, aiming to clean out zinc acetate from powders. Very structured EXAFS spectra are obtained after washing: EXAFS spectra of samples which were previously identified as belonging to Family I are now totally superimposable to the one of the crystalline ZnO reference, whereas those of samples identified in the Family II display a shape similar to the EXAFS spectrum of the synthesized acetate Zn−HDS sample.

4. Discussion

The analysis of the long and local range order for each family of precipitate is enlightening to understand the complex chemistry associated with the formation of solids by hydrolysis of zinc acetate derivative in ethanolic solution. The diffraction patterns and thermal analysis results show that whatever the catalyst used, the powders so obtained by hydrolysis are always a mixture of several phases. Contrary to the diffraction for which it is difficult to extract—without preliminary preparation—a quantitative composition dealing with a mixture of phase, the EXAFS technique is well suited to determine the proportion of the different components in the mixture providing that the EXAFS signals of the individual components are known. The removal of zinc acetate species by washing, for some of the samples, leads to a "pure" nanocrystalline ZnO phase and a "pure" nanocrystalline acetate Zn-HDS phase as evidenced in Figure 5. The EXAFS spectra of these single phases and that corresponding to the initial $ZnAc_2 \cdot 2H_2O$ reagent were combined in different proportions to be compared to the EXAFS spectra of the powdered samples. It first appears from this comparison

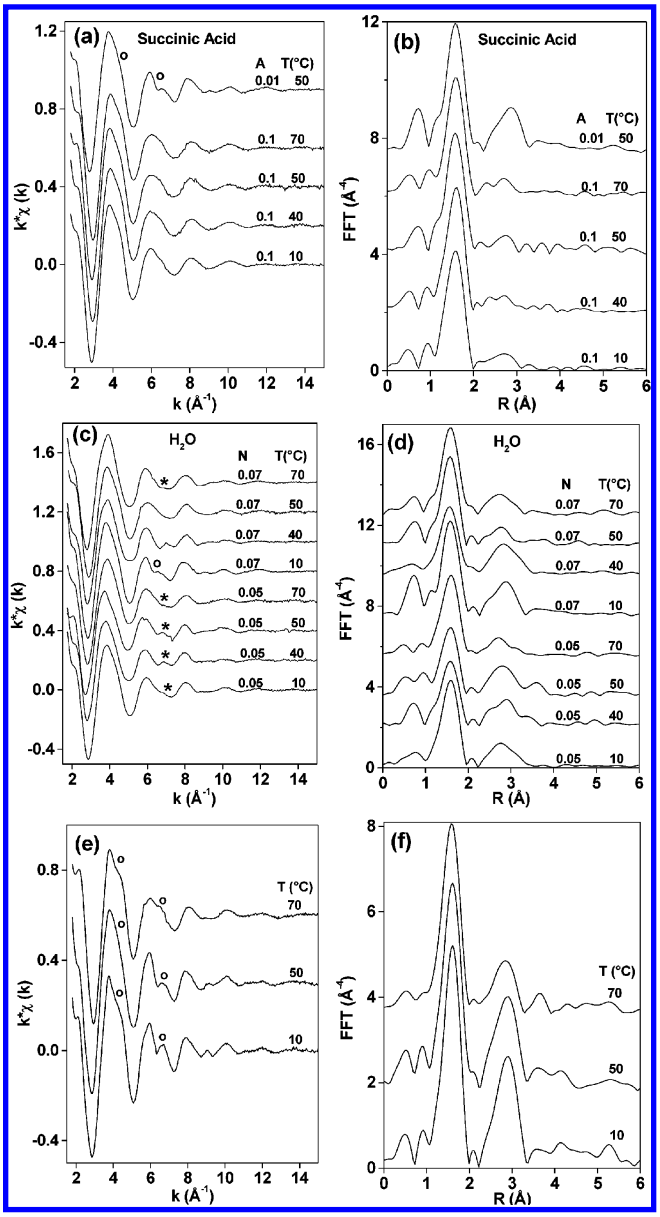

Figure 4. EXAFS spectra (left side) and corresponding FT (right side) of the precipitates obtained with the reaction bath at different temperatures. (a) and (b) After the addition of succinic acid with the molar ratio $A = 0.1$ and $A = 0.01$, (c) and (d) after the addition of water with the molar ratio $N = 0.05$ and $N = 0.07$, (e) and (f) without addition of water and catalyst. The circles mark some fingerprints of Family I, whereas the stars are related to those of Family II.

that the more likely combinations are always obtained with at least 40% of $ZnAc_2 \cdot 2H_2O$ in the mixture. Second, the arbitrary distinction into three families made from the EXAFS data indeed results from different proportions of the three compounds in the mixture. The proportions obtained by using different linear combinations are gathered in Table 2. Examples of comparisons of these combinations with the experimental spectra of some precipitates are given in Figure 6.

For clarity, we will first discuss the local range order around Zn for each family. Then, we will analyze the effect of temperature, addition of water, and of catalyst on the formation of different zinc-based compound.

4.1. Zn-Local Structure in Different Families. *Family I.* On one hand, the EXAFS spectra of samples belonging to the Family I (Figures 2 and 4) look like the spectra recombined from the highest amount of ZnO nanoparticles (Figure 6). This

TABLE 2: Classification of the Solids into Three Families of Compounds Labeled I, II, and III (see the text)

Temp °C	LiOH B=0.1	Succinic A=0.01	Succinic A=0.1	Acetic A=0.1	H_2O N=0.05	H_2O N=0.07	Without Catalysis
10	35% 0% 65%*	X	1% 0% 99% 1.99 1.82	X	5% 20% 75%	15% 0% 85% 2.14 2.30	30% 0% 70% 2.10 2.81
40	0% 60% 40%* 2.15 2.38	X	0% 0% >99% 2.99 1.78	10% 10% 80% 2.06 2.23	0% 50% 50% 2.25 2.27	0% 50% 50%*	X
50	0% 40% 60% 2.12 2.18	15% 0% 80%	0% 0% >99% 2.08 1.78	20% 0% 80% 2.10 2.47	5% 35% 60% 2.21 2.30	5% 20% 75% 2.23 2.15	30% 20% 50% 2.15 3.00
70	0% 0% >99% 2.28 1.78	X	0% 0% >99% 2.32 1.78	10% 30% 60% 2.22 2.43	0% 20% 80% 2.03 1.98	0% 20% 80%	1% 0% 99%
	Family: I	II	III				

[a] Crosses Indicate that the solid has not been prepared, whereas the asterisk (*) means that the sample has been also characterized after washing by distilled water. The proportions between ZnO, Zn-HDS, and zinc acetate obtained by EXAFS are indicated in this sequence in the top of each field. The measured densities and the theoretical densities calculated from linear combinations of single crystal densities of each phase (ρ ($ZnAc_2.2H_2O$) = 1.786 g/cm^3, ρ (ZnO) = 5.2 g/cm^3, and ρ (Zn-HDS) = 2.78 g/cm^3) according to the proportion determined from EXAFS data are shown in the bottom of the field in the left and right corners, respectively.

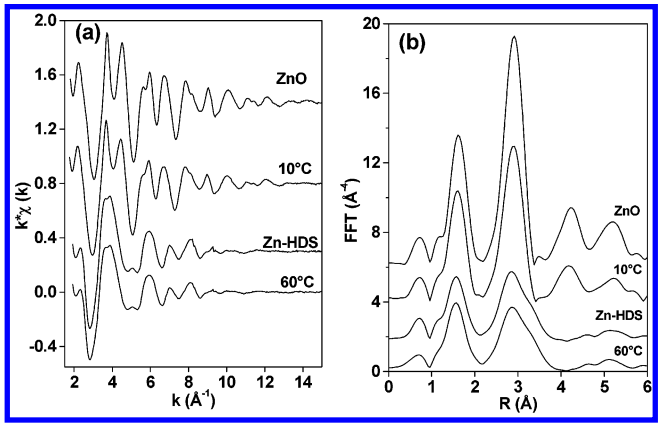

Figure 5. (a) EXAFS spectra of powders prepared by LiOH catalysis at 10 °C and 60 °C after washing with distilled water, and (b) corresponding FT of the EXAFS signals displayed in (a). For comparison purpose, the EXAFS signals of the ZnO and $Zn_5(OH)_8(OCOCH_3)_2 \cdot 2H_2O$ (Zn-HDS) references have been also reported.

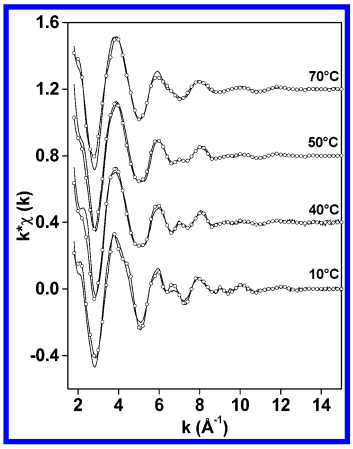

Figure 6. Comparison of the reconstructed EXAFS signals (marked by circles) from linear combinations of spectra of nanocrystalline ZnO, nanocrystalline acetate Zn-HDS, and zinc acetate starting reagent with typical EXAFS spectra (full line) of samples belonging to each family reported in Table 1.

result is first supported by the structural parameters of the first coordination shell (4 ± 0.2 oxygen atoms at 2.01 ± 0.01 Å, see Table 1) determined by the least-squares fitting procedure.

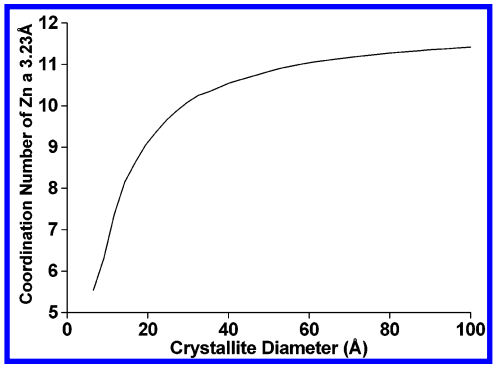

Figure 7. Theoretical correlation between the mean coordination number of zinc atoms at 3.23 Å in ZnO and the nanocrystalline size of the ZnO cluster. The theoretical approach used herein is similar to that described in ref 20.

Second, the lack of intense lines for $2\Theta < 10°$ on the XRPD patterns of these samples strongly indicates that the proportion of the acetate Zn-HDS phase in the mixture is small. These samples are mainly composed of a mixture of ZnO and $ZnAc_2 \cdot 2H_2O$. The comparison of the experimental data (Figures 2 and 4) with the recombined EXAFS spectra (Figure 6) made from ZnO and $ZnAc_2 \cdot 2H_2O$ gives a composition in ZnO ranging from 10 to 35%. The mixture of ZnO and $ZnAc_2 \cdot 2H_2O$ phases explains the difficulty in fitting the second peak of the FTs of the different samples of this family. A good fit was achieved only in the case of the "pure" nanocrystalline ZnO phase obtained after washing the sample issued from a catalysis at 10 °C by LiOH. The coordination number obtained for the Zn second nearest neighbors (at 3.23 ± 0.02 Å) is of about 8.4 ± 0.6. According to the correlation of this coordination number and the nanocrystalline size established theoretically[20] for the ZnO network (Figure 7) the diameter of the ZnO particles was estimated from the EXAFS results to about 1.6 ± 0.6 nm. This result is totally in agreement with the size of primary particles determined by small-Angle X-ray scattering (SAXS).[21]

Family II. The shape of the EXAFS spectra (Figures 2 and 4) characteristic of samples belonging to the Family II is satisfactorily reproduced by the combinations richest in the Zn-HDS phase. This is in agreement with the use of a two shell fitting procedure for the first coordination shell (Table 1): one with oxygen atoms at 2.02 ± 0.02 Å as in ZnO and the other

oxygen at longer distances located around 2.15−2.18 ± 0.02 Å. As reported in the literature for $ZnAc_2{\cdot}2H_2O$[22] and HDS phases based on zinc[16−18] these latter distances are characteristic of an octahedral environment around the absorbing Zn atom. The proportion of the Zn-HDS phase in these samples ranges from 20 to 60%, whereas the amount of ZnO is small, typically around 5% or less.

Family III. The shape of the EXAFS spectra characteristic of samples belonging to Family III (Figure 4) is reproduced by linear combinations in which the total proportion of ZnO and Zn-HDS phases does not exceed 5% (Table 2). The samples without the HDS phase involved in their compositions, e.g., the samples obtained at 70 °C from catalysis by succinic acid or without catalysis, present accordingly diffraction patterns free of the intense line for $2\Theta < 10°$.

For some of the samples, measured densities are compared in Table 2 to the values calculated from linear combinations of densities of each "pure" compound using the proportions obtained by EXAFS analysis. A satisfactory agreement is achieved for samples belonging to families I and II prepared from water and LiOH catalysis. This validates the proposed proportions of each phase in the mixture.

4.2. Effect of the Temperature and of the Catalyst. Precipitates obtained by using succinic acid ($A = 0.1$) catalyst present a relatively constant local order around Zn at the different temperatures of preparation, characterized by very small amounts of ZnO and Zn-HDS phase. This results from two concomitant effects, which simultaneously reduce the condensation rate of precursors into ZnO particles. First, the strong chelating power of succinic acid which is present at high concentration can improve the hydrolytic stability of the precursors. Second, acid media[23] improves the solubility of ZnO in ethanolic solution. Then the little amount of ZnO which has precipitated, despite the unfavorable complexing conditions, can be redissolved in such acid media. These interpretations are well corroborated by the fact that for the lowest concentration in succinic acid ($A = 0.01$) it was possible to obtain precipitates belonging to Family I, i.e., characterized by about 10 to 35% of ZnO. In this case, because of the low concentration of complexing agent, the hydrolysis and condensation reactions could occur toward the formation of the oxide network.

Samples prepared from LiOH ($B = 0.1$) catalysis are very sensitive to the synthesis temperature. The best condition to obtain the higher proportion of ZnO nanoparticles in the solid phases mixture is a synthesis carried out at 10°C. This result is totally in agreement with the observation made by Spanhel and co-workers[4] as well by other groups,[8−10] which recommend low temperatures (between 0 and 20 °C) for the preparation of ZnO nanoparticles. Nevertheless, the formation rate is slower than at higher temperature as shown by the isothermal measurements of turbidity as a function of time.[11] Our results (Table 2) indicate that the increase of the temperature favors the formation of the Zn-HDS in the mixture, the higher amount being reached at 40 °C. Finally, for the samples prepared at 70 °C, precipitates obtained are mainly composed of unreacted zinc acetate powder leading to a poor yield in the formation of zinc oxide and/or Zn-HDS powders. As the solubility of ZnO nanoparticles increases with the temperature,[8] this feature indicates that the relative amount of compounds in the precipitate depends on the concentration of zinc-dissolved species.

To our best knowledge, the identification of the acetate Zn-HDS phase as a subproduct of the Spanhel and Anderson[4] derived method to prepare ZnO nanoparticles has never been reported in the literature. In fact, as evidenced in Figure 1, the identification of the nanoparticulate acetate Zn-HDS phase can be done only on the basis of its (00*l*) reflection located at $2\Theta \approx 6°$. Because no peaks are expected for hexagonal ZnO crystallites below $2\Theta = 30°$ (for a Cu Kα radiation), the few X-ray patterns of isolated powders are usually reported in the literature[4,24] for $2\Theta \geq 30°$. Meulenkamp was the only one which has reported extended X-ray patterns[8] and according to the present work, precipitates obtained by adding heptane to as-prepared fresh sols within 1 day after preparation present a diffraction peak located at small 2Θ. No detailed elucidation of the structure and composition of this precipitate was attempted,[8] but according to the results reported herein we attribute this peak to the presence of the Zn-HDS phase. How such Zn-HDS sub-product is formed is an intriguing question. Frequently, HDS compounds are prepared in aqueous media from the slow addition of NaOH into a solution of the zinc salt[12] or by reacting ZnO powder with a zinc salt in solution.[25] Recently,[26] a new method was reported for preparing layered hydroxide metal acetates (metal = zinc, cobalt, and nickel) based on hydrolysis at room temperature, in polyol or alcohol medium, of supposed alkoxyacetate precursors. In ethanol media the synthesis conditions are very close to those used in this work: first the hydrated zinc acetate (0.1 mol L^{-1}) is dissolved in ethanol at 76 °C followed by the addition of an excess of water ($N = 2$) at room temperature to induce hydrolysis process.

The experimental conditions for the first route are encountered by using LiOH catalysis. A competition between the hydrolysis condensation of molecular Zn^{2+} precursors into ZnO and Zn-HDS occurs in such basic media. These solid phases can be formed independently as suggested by the stepped kinetic of particle growth observed in situ by SAXS[21] during the synthesis at 40 °C in the presence of LiOH. In the first step, an increase of the number of small particles with 2 nm in diameter occurs which are now identified by EXAFS as ZnO nanoparticles. In the second step, a growth of a second family of particles with a diameter ranging from 5 to 7 nm is observed. The chemical nature of the particles of this second family was not identified, but on the basis of the results presented herein, we assume that they are constituted by the acetate Zn-HDS phase.

The synthesis of acetate Zn-HDS phase reported in the literature[25] following the second method in aqueous media proceeds by aging ZnO powder into a zinc acetate solution in stoichiometric proportion for 24 h at room temperature. In this case the formation of the HDS phase results from a redissolution process of ZnO leading to the coexistence of dissolved Zn^{2+} species in the presence of unreacted $Zn(Ac)_2{\cdot}2H_2O$ and $Zn_4O(Ac)_6$ precursors. This redissolution was evidenced by in situ SAXS measurements[27] during the synthesis at 60 °C in the presence of water ($N = 0.05$). The two families of particles discussed above in the case of basic catalysis at 40 °C are already formed. But the smallest ZnO particles, which are first formed, are consumed with time whereas the second larger ones appear. We assume that the formation of the second family of particles results from a mechanism of dissolution/reprecipitation of ZnO nanoparticles.

Finally, we should mention that the formation of an acetate-HDS phase mixed with $Zn(Ac)_2{\cdot}2H_2O$ was also observed in the precipitate obtained after solvent evaporation at room temperature under reduced pressure of the initial precursor solution (without water and catalyst additions).This feature is evidenced by EXAFS and XRPD data shown in Figure 8, where the proportion of $Zn(Ac)_2{\cdot}2H_2O$ and Zn-HDS phases deduced from EXAFS results is 60%:40%, respectively. It indicates that a part of the total amount of acetate Zn-HDS find in the isolated powder (Table 2) could be formed during drying of the

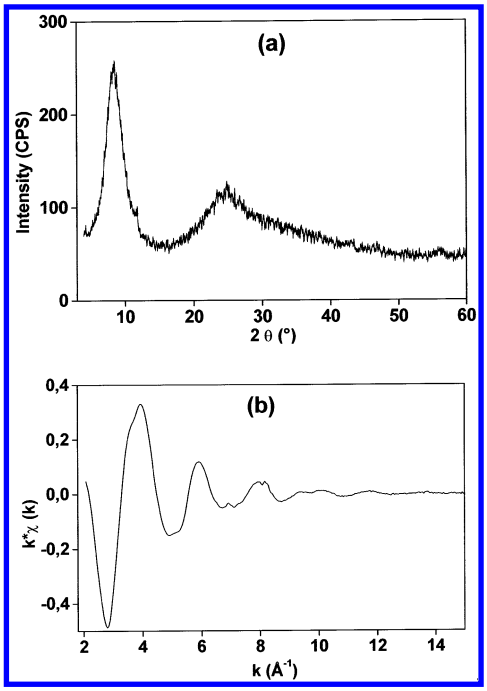

Figure 8. (a) XRPD pattern and (b) EXAFS spectrum of the powder extracted from the precursor solution by solvent evaporation at room temperature under reduced pressure.

precipitated paste. The influence of drying on the control of the proportion of the different species is under study.

In summary, our results reveal that the formation of Zn-HDS phase results from several processes in which pH and temperature play a key role. In the 40−60 °C temperature range, these processes give rise to the higher proportion of acetate Zn-HDS in the mixture of phases extracted from the sols. Below this temperature range, the solubility of ZnO into EtOH is small, giving rise to Family I, in which the amount of ZnO is large. Above this temperature range, the high solubility of ZnO leads to the dominant presence of zinc acetate. An analogous behavior occurs by changing the pH from basic to acid and by addition of water. It can increase the concentration of dissolved Zn^{2+} species, as zinc salts are generally more soluble in water than in ethanol and in acidified solution. Furthermore, it is well-known that the pH has a strong effect on the kinetics of hydrolysis and condensation reactions involved in sol−gel chemistry.[2] The hydrolysis is faster at low pH, while higher pH induces faster condensation.[2] Thus the relative amount of each zinc phase in the powder depends on the equilibrium between hydrolysis−condensation and complexation (dissolution)−reprecipitation reactions.

Finally, the dependence of the relative amount of ZnO nanoparticle and Zn-HDS on the synthesis conditions, associated with the possibility of reduced zinc acetate content in the precipitate by washing, allows the best understanding of changes in particle morphology of fired ZnO powder reported in the literature.[8−11] On one hand, the layered structure of the HDS compounds favors the growth of placket-shaped particles. This morphology is preserved during the topotatic transformation of Zn-HDS in ZnO by controlled firing.[12,28] On the other hand, spherical nanoparticles are obtained when the synthesis condition leads to the dominant formation of ZnO colloidal particles.

5. Conclusions

The chemical and structural nature of powders prepared from the zinc acetate sol−gel route is highly dependent on the temperature and nature of catalyst used in the hydrolysis step. All the powders are composed of a mixture of zinc oxide (ZnO), zinc acetate ($ZnAc_2 \cdot 2H_2O$), and zinc hydroxyacetate (Zn-HDS), and their relative amounts can be controlled by the fine-tuning of the sol−gel synthesis parameters. Powders with the highest amount of ZnO are usually obtained at low synthesis temperature (<20 °C) without catalyst or using LiOH as basic catalyst. The $ZnAc_2 \cdot 2H_2O$ can be eliminated by washing with water, leading to powders mainly formed by 1.6 ± 0.6 nm sized ZnO nanoparticles. Powders with the highest proportions of acetate Zn-HDS phase are obtained near 40 °C under basic catalysis or by water addition ($N = 0.05$ or 0.07). In the presence of succinic acid ($A = 0.1$, $T = 10-70$ °C) the $ZnAc_2 \cdot 2H_2O$ is the main component of powders.

The formation of the acetate Zn-HDS from this sol−gel route pointed out in this work results from a mechanism of dissolution/reprecipitation of ZnO nanoparticles. The marked dependence of the relative amount of these compounds on the synthesis conditions can be useful to in the preparation of ZnO particles with controlled morphology, i.e., spherical and plate-shaped.

Acknowledgment. The authors acknowledge the collaboration of LURE staff during the EXAFS experiments and the financial support from Brazilian (CAPES and FAPESP) and French (COFECUB) agencies.

References and Notes

(1) Cohen, M. L. *Annu. Rev. Mater. Sci*. **2000**, *30*, 1.
(2) Brinker, C. J.; Scherer, G. W. *Sol−Gel Science: The Physics and Chemistry of Sol−Gel Processing*; Academic Press: San Diego, 1990.
(3) Livage, J.; Henry, M.; Sanchez, C. *Prog. Solid State Chem.* **1988**, *18*, 259.
(4) Spanhel, L.; Anderson, M. A. J. *Am. Chem. Soc.* **1991**, *113*, 2826.
(5) Redmond, G.; Fitzmaurice, D.; Graetzel, M. *Chem. Mater.* **1994**, *6*, 686.
(6) Tokumoto, M. S.; Pulcinelli, S. H.; Santilli, C. V.; Briois, V. *J. Sol-Gel Sci. Technol.* **2003**, *26*, 547.
(7) Hiltunen, L.; Leskela, M.; Makela, M.; Niinisto, L. *Acta Chem. Scand. A* **1987**, *41*, 548.
(8) Meulenkamp, E. A. *J. Phys. Chem. B* **1998**, *102*, 5566.
(9) Sakohara, S.; Tickanen, L. D.; Anderson, M. A. *J. Phys. Chem.* **1992**, *96*, 11086.
(10) Sakohara, S.; Ishida, M.; Anderson, M. A. *J. Phys. Chem.* **1998**, *102*, 10169.
(11) Tokumoto, M. S.; Pulcinelli, S. H.; Santilli, C. V. *Advances in Science and Technology, Ceramics: Getting into the 2000's − Part B*; Vincenzini, P., Ed.; Techna Srl, 1999; p 73.
(12) Morioka, H.; Tagaya, H.; Karasu, M.; Kadokawa, J. I.; Chiba, K. *J. Mater. Res.* **1998**, *13*, 848.
(13) Michalowicz, A. *EXAFS pour le Mac, Logiciels pour la Chimie*; Société Française de Chimie: Paris, 1991; p 102.
(14) Abraham, S. C.; Bernstein, J. L. *Acta Crystallogr. B* **1969**, *25*, 1233.
(15) . Mustre de Leon, J.; Rehr, J. J.; Zabinsky, S. I.; Albers, R. C. *Phy. Rev. B* **1991**, *44*, 4146.
(16) Stählin, W.; Oswald, H. R. *Acta Cryst. B* **1970**, *26*, 860.
(17) Allmann, R. *Z. Kristallogr.* **1968**, *126*, 417.
(18) Ghose, S. *Acta Crystallogr.* **1964**, *17*, 1051.
(19) Koga, N.; Tanaka, H. *Thermochim. Acta* **1997**, *303*, 69.
(20) Briois, V.; Santilli, C. V.; Pulcinelli, S. H.; Brito, G. E. S. *J. Non-Cryst. Solids* **1995**, *191*, 17.
(21) Tokumoto, M.; Pulcinelli, S. H.; Santilli, C. V.; Craievich, A F. *J. Non-Cryst. Solids* **1999**, *247*, 176.
(22) Ishioka, T.; Murata, A.; Kitagawa, Y.; Nakamura, K. T. *Acta Cryst. C* **1997**, *53*, 1029.
(23) Meulenkamp, E. A. *J. Phys. Chem. B* **1998**, *102*, 7764.
(24) Wong, E. M.; Bonevich, J. E.; Searson, P. C. *J. Phys. Chem. B* **1998**, *102*, 7770.
(25) Mey, M.; Beneke, K.; Lagaly, G. *Inorg. Chem.* **1993**, *32*, 1209.
(26) Poul, L.; Jouini, N.; Fiévet, F. *Chem. Mater.* **2000**, *12*, 3123.
(27) Tokumoto, M.; Pulcinelli, S. H.; Santilli, C. V.; Craievich, A. F.; Baudelet, F.; Dartyge, E.; Briois, V. Manuscript in preparation.
(28) Morioka, H.; Tagaya, H.; Karasu, M.; Kadokawa, J. I.; Chiba, K. *Inorg. Chem.* **1999**, *38*, 4211.